Journal of Materials Chemistry A

PAPER

View Article Online
View Journal | View Issue

Cite this: J. Mater. Chem. A, 2016, 4, 8350

Factors affecting cycling life of $LiNi_{0.8}Co_{0.15}Al_{0.05}O_2$ for lithium-ion batteries†

Yoshinari Makimura,* Tsuyoshi Sasaki, Takamasa Nonaka, Yusaku F. Nishimura, Takeshi Uyama, Chikaaki Okuda, Yuichi Itou and Yoji Takeuchi

Received 10th February 2016
Accepted 19th April 2016

DOI: 10.1039/c6ta01251e

www.rsc.org/MaterialsA

Factors affecting the cycling life of cylindrical lithium-ion batteries of $LiNi_{0.8}Co_{0.15}Al_{0.05}O_2$ (NCA) with graphite were examined in terms of the rechargeable capacity and polarization of NCA derivatives of $Li_zNi_{0.8}Co_{0.15}Al_{0.05}O_{2-\delta}$ ($0.8 \leq z \leq 1.05$). NCA derivatives with rock-salt domains in the structure were prepared by a co-precipitation method and the structures of $[Li_{1-y}Ni_y]^{3(b)}[Ni,Co,Al]^{3(a)}O_2{}^{6(c)}$ based on a space group of $R\bar{3}m$ were refined by a Rietveld method of the XRD patterns. The electrochemical reactivity of the NCA derivatives with rock-salt domains was examined in non-aqueous lithium cells, and it was found that the rechargeable capacities (Q) of the samples decrease linearly as the amount of rock-salt domain (y) increases. An empirical relation is obtained to be $Q = 181.4 - 725.5y$ in which Q reaches zero at $y = 0.25$, which is derived from not only the capacity loss owing to inactive rock-salt domains but also the polarization increase. The galvanostatic intermittent titration technique (GITT) measurement told us that polarization of NCA derivatives increases when the amount of rock-salt domains is above 2%, *i.e.*, $y > 0.02$, and such a relation is remarkable in the lithium insertion direction into the structure, which is ascribed to slow lithium ion mobility due to nickel ions in the lithium layers. The NCA derivatives with increased rock-salt domains of above 2% deteriorate rapidly in non-aqueous lithium cells upon charge and discharge cycles, which is ascribed to the cumulative increase in polarization during charge and discharge. An extended cycling test for cylindrical lithium-ion batteries of the NCA derivatives with a graphite negative electrode at elevated temperature was performed and the quantitative relation is discussed thereof.

Introduction

Lithium-ion batteries, which were designed as power sources for portable devices such as mobile phones and notebook computers, have been applied to large-sized energy storage devices for automotive and stationary purposes.[1–4] For large-sized applications, positive electrode materials of manganese, iron, and/or nickel species have to be used rather than $LiCoO_2$ with respect to a low risk for the resource crisis. Of these, $LiNiO_2$-based materials are attractive because of a large rechargeable capacity of more than 150 mA h g^{-1}, a moderately high operating voltage above 3.6 V *vs.* Li, and a characteristic S-shaped curve over the entire range of operation.[5,6] The required performances of lithium-ion batteries for large-sized applications are quite challenging for researchers and engineers with respect to durability and safety, and hence operating conditions for lithium-ion batteries have to be monitored and be strictly controlled in terms of temperature, voltage and current to overcome these concerns.[7–12] Deterioration of lithium-ion batteries by extended cycling or storage tests especially at elevated temperature has been reported by many research groups to be attributed to the degradation of positive electrode materials such as $LiNi_{0.8}Co_{0.15}Al_{0.05}O_2$ (NCA) in a microscopic or macroscopic scale.[11–22] Degradation of the NCA-based positive electrode has been examined with respect to the increase in interfacial resistance at the positive electrode,[13,17] generated micro-cracks in the particles,[11,12] or formation of NiO-like rock-salt domains.[11,12,15,16,22] The similarity of reaction products between exothermic reactions of positive electrode materials at high temperature above 150 °C and material degradation during cycling at 60 °C strongly suggests that positive electrode materials are key for tough and safe batteries.[23–26] Our group has also reported the deterioration of lithium-ion batteries of NCA with graphite during extended cycling for more than 500 cycles at an elevated temperature above 60 °C, derived from the localized degradation of NCA to form NiO-like rock-salt domains in the structure.[20,21] Electrochemical impedance spectroscopy (EIS) measurement of the 500 mA h class cylindrical lithium-ion batteries of NCA with graphite revealed that the rise in internal

Toyota Central Research and Development Laboratories, Incorporated, Nagakute, Aichi 480-1192, Japan. E-mail: ymakimura@mosk.tytlabs.co.jp

† Electronic supplementary information (ESI) available: Summary on the compositions of the samples determined by ICP-AES, SEM images, Co K-edge XANES spectra, intermittent charge and discharge curve, and voltage profiles in a lithium cell. See DOI: 10.1039/c6ta01251e

resistance of the batteries was dominated by the rise in the charge-transfer resistance of the positive electrode, which corresponds to the right semicircle resistance in the lower frequency range in the Nyquist plots of two semicircles.[19] Temperature dependence of the charge-transfer resistance of NCA before and after the cycling test indicated that the impedance rise of the NCA positive electrode was caused by a reduction in the number of active sites for the charge-transfer process, hence NiO-like rock-salt domains localized at the surface of the NCA particles were considered to be inactive to reduce the number of active sites.[27] Electrochemical reactivity of the rock-salt domains is actually not obvious and the relation between the formation of rock-salt domains and the deterioration of lithium-ion batteries has not been quantitatively understood because only trace amounts of rock-salt domains are generated after extended cycling at elevated temperature. In this paper, NCA derivatives of $Li_zNi_{0.8}Co_{0.15}Al_{0.05}O_{2-\delta}$ ($0.8 \leq z \leq 1.05$) having quantitatively-controlled rock-salt domains in the structure were prepared and electrochemical measurements were performed to clarify the relationship between the rock-salt domains and electrochemical reactivity in terms of the rechargeable capacity and polarization. An extended cycling test of the 500 mA h class cylindrical lithium-ion batteries of NCA derivatives was also performed, and a possible way to improve battery performance is discussed thereof.

Experimental

A co-precipitation method was applied to prepare $Li_zNi_{0.8}Co_{0.15}Al_{0.05}O_{2-\delta}$ samples. A mixed solution of nickel, cobalt, and aluminum nitrates and an aqueous solution of lithium hydroxide were dripped simultaneously into a stirred flask. For the reaction product to be a precipitate it was washed several times with distilled water, and dried at 80 °C for 12 hours. The obtained powder of nickel, cobalt, and aluminum species was mixed with lithium carbonate, and the reaction mixture was heated at 750 °C under an oxygen stream. The value of z in $Li_zNi_{0.8}Co_{0.15}Al_{0.05}O_{2-\delta}$ was adjusted by the molar ratios of lithium to nickel, cobalt, and aluminum ions in the starting materials.

The obtained samples of $Li_zNi_{0.8}Co_{0.15}Al_{0.05}O_{2-\delta}$ were characterized by powder X-ray diffraction using a RINT-TTR II powder diffractometer (Rigaku Corp., Japan) with Cu Kα radiation, and a Rietveld method using the GSAS package with the EXPGUI interface[28] based on the structural model of $[Li_{1-y}Ni_y]^{3(b)}[Ni,Co,Al]^{3(a)}O_2{}^{6(c)}$ assuming a space group of $R\bar{3}m$.

The X-ray absorption spectral measurements of $Li_zNi_{0.8}Co_{0.15}Al_{0.05}O_{2-\delta}$ were carried out at a BL33XU beam line in SPring-8. A Si(111) channel-cut crystal monochromator was used for incident X-rays, and harmonic contamination of the beam was prevented using a Rh-coated Si mirror. The intensities of the incident and transmitted X-rays were measured by the ion chamber detectors at room temperature.

The electrochemical behavior of $Li_zNi_{0.8}Co_{0.15}Al_{0.05}O_{2-\delta}$ was examined using the sandwich-type electrochemical cell of Type TJ-AC (Tomcell Co. Ltd., Japan) with a lithium foil supported on a stainless steel plate as the negative electrode. The positive and negative electrodes separated by a microporous polypropylene film were immersed in 1 M $LiPF_6$ ethylene carbonate (EC)/dimethyl carbonate (DMC)/ethyl methyl carbonate (EMC) (3/4/3; volume ratio) electrolyte. 500 mA h class cylindrical lithium-ion batteries consisting of wound sheets of the $Li_zNi_{0.8}Co_{0.15}Al_{0.05}O_{2-\delta}$ positive electrode and graphite negative electrode with a microporous polypropylene film were also fabricated to examine the cycling stability at an elevated temperature of 60 °C. A black viscous slurry of the positive electrode mix consisting of 85 wt% $Li_zNi_{0.8}Co_{0.15}Al_{0.05}O_{2-\delta}$, 10 wt% carbon black, and 5 wt% polyvinylidene fluoride (PVdF) binder dissolved in *N*-methyl-2-pyrrolidone (NMP) was painted on one side of an aluminum foil for the electrochemical cell or on both sides for the cylindrical lithium-ion batteries, and was dried under vacuum at 120 °C for 12 h. The painted sheets were pressed to increase the electrode density and cut to be the positive electrodes. The graphite negative electrodes were prepared in the same way as the positive electrode, which consists of 95 wt% graphite and 5 wt% PVdF binder coated on copper foil.

The electrochemical cells were operated in a galvanostatic mode at C/10-rate in a voltage window of 4.2–2.5 V at 20 °C to examine the electrochemical reactivity of $Li_zNi_{0.8}Co_{0.15}Al_{0.05}O_{2-\delta}$. Intermittent charge and discharge measurement in a galvanostatic intermittent titration technique (GITT) mode of the electrochemical cells was performed at C/10-rate at 20 °C. The cell operation was interrupted every 10 mA h g^{-1}, and re-started when the voltage slope was below 1 mV h^{-1}.

The extended cycling test for the cylindrical lithium-ion batteries of NCA derivatives with the graphite negative electrode was performed for 500 cycles at an elevated temperature of 60 °C in a voltage range of 4.1–3.0 V at 2C-rate.

Results and discussion

Preparation of $LiNi_{0.8}Co_{0.15}Al_{0.05}O_2$ derivatives with rock-salt domains

In order to prepare NCA derivatives with rock-salt domains, the ratios of lithium to metal ions in the starting materials were adjusted to be $z = 1.05$, 1.02, 1.00, 0.98, 0.95, 0.90, and 0.80 in $Li_zNi_{0.8}Co_{0.15}Al_{0.05}O_{2-\delta}$, and X-ray diffraction (XRD) patterns of the obtained samples are displayed in Fig. 1. The chemical compositions of the samples were determined by inductively coupled plasma-atomic emission spectroscopy (ICP-AES), and are listed in Table S1.† The lithium amounts listed in Table S1† are 2–3% less than the z values, which are acceptable since these values can be explained by the 2–3% lithium evaporation during the heating process at 750 °C in preparation. The morphologies of the NCA derivatives ($z = 1.05$, 0.90, and 0.80) were observed by scanning electron microscopy (SEM) and are displayed in Fig. S1.† Irrespective of the chemical compositions of the NCA derivatives, the samples were comprised of large agglomerates of about 20 μm, which were composed of small particles of 0.5–1.5 μm in size. $Li_zNi_{0.8}Co_{0.15}Al_{0.05}O_{2-\delta}$ samples give XRD patterns of the single phase associated with the rhombohedral lattice, and hence miller indexes are given in the hexagonal

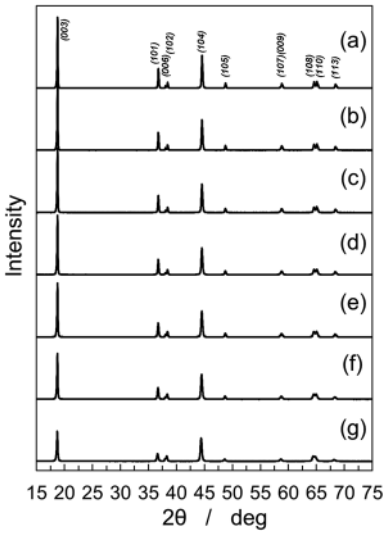

Fig. 1 XRD patterns of $Li_zNi_{0.8}Co_{0.15}Al_{0.05}O_{2-\delta}$ prepared by adjusting the Li/M ratios (M: $Ni_{0.8}Co_{0.15}Al_{0.05}$) of z = (a) 1.05, (b) 1.02, (c) 1.00, (d) 0.98, (e) 0.95, (f) 0.90, and (g) 0.80.

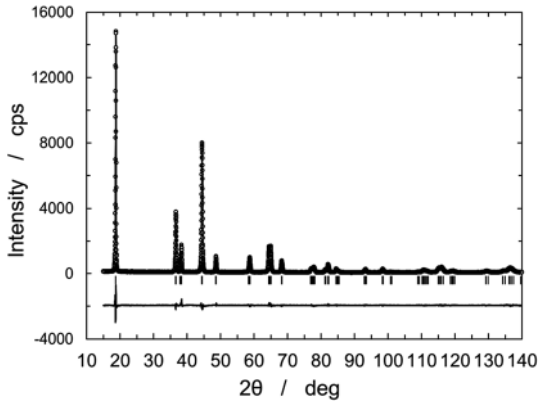

Fig. 2 Rietveld analytical result on $Li_zNi_{0.8}Co_{0.15}Al_{0.05}O_{2-\delta}$ (z = 0.90) assuming a space group of $R\bar{3}m$. Open circles indicate the observed intensity and a solid curve indicates the calculated pattern using the parameters listed in Table 1. The difference between the observed and calculated patterns is shown at the bottom.

setting. Of these, $Li_zNi_{0.8}Co_{0.15}Al_{0.05}O_{2-\delta}$ (z = 1.05; NCA) shown in Fig. 1(a) exhibits a large diffraction peak of (003) in comparison to that of (104) and a clear peak split of (006)/(102) or (108)/(110) in the XRD pattern, which indicates that $Li_zNi_{0.8}Co_{0.15}Al_{0.05}O_{2-\delta}$ (z = 1.05) has an α-$NaFeO_2$-type layered structure. As the z value in $Li_zNi_{0.8}Co_{0.15}Al_{0.05}O_{2-\delta}$ decreases from 1.05 to 0.8, the (006) peak shifts to a higher diffraction angle toward the (102) peak, and the (110) peak approaches the (108) peak in its location. The (003) peak intensity decreases while that of (104) keeps a constant value. Such changes in the peak intensity and location are ascribed to increased transition metal ions especially nickel ions at the lithium layers in the α-$NaFeO_2$-type layered structure.[6,29] In NCA derivatives prepared in this work, the rock-salt domains should be uniformly distributed in the lithium layers. Scanning transmission electron microscopy (STEM) will give us more insight into the distribution of nickel ions in the lithium layers as has been reported in our previous papers.[30,31] Such an approach is in progress in our research group. Rietveld analyses of the XRD patterns of the $Li_zNi_{0.8}Co_{0.15}Al_{0.05}O_{2-\delta}$ ($0.8 \le z \le 1.05$) samples were performed by assuming the structural model of $[Li_{1-y}Ni_y]^{3(b)}[Ni,Co,Al]^{3(a)}O_2{}^{6(c)}$ based on a space group of $R\bar{3}m$. The Rietveld analytical results on the sample of z = 0.90 are shown in Fig. 2 and the analytical results on those of $0.8 \le z \le 1.05$ are summarized in Table 1. Oxygen positional parameters of Z_{ox} are 0.2591–0.2598, which are consistent with previous results.[5,32,33] The y value is estimated to be 0.0023 at z = 1.05, and increases to 0.1280 at z = 0.8. The values of $(1-y)/(1+y)$ were calculated to confirm the validity of the analysis, which should be comparable to the z value in $Li_zNi_{0.8}Co_{0.15}Al_{0.05}O_{2-\delta}$. As listed in Table 1, $(1-y)/(1+y)$ values are 2–3% less than the z values, which are comparable to the analytical results by ICP-AES listed in Table S1.† The y values of the samples of z = 1.05 and 1.02 are positive numbers in spite of the lithium excess amount of z > 1.0 in preparation of the samples, which indicates that $LiNiO_2$-based materials do not have lithium ions in transition metal layers as reported by Delmas' research group.[6,33] Such a phenomenon is not the case for $Li(Ni,Co,Mn)O_2$ positive electrode materials since layered lithium manganese oxides can accommodate lithium ions in transition metal layers like Li_2MnO_3 (or $Li[Li_{1/3}Mn_{2/3}]O_2$ in a layered formulation).[34–36] The hexagonal cell parameters, a and c, increase and the c/a ratio decreases as the y value increases as listed in Table 1. The c/a ratio of the cubic symmetry should be about 4.899, and hence the change in the c/a ratios from 4.95 to 4.94 indicates the change in symmetry from rhombohedral toward a cubic lattice. The a-axis parameter is the edge distance of the unit octahedron MO_6 (M: Ni, Co, Al), which reflects the change in bond length of M–O, since the combination of a MO_6 octahedron gives a two-dimensional layer forming the triangular lattice of sites.[37] The increase in the a-axis parameter indicates that the M–O bond length increases, which is ascribed to the reduction of transition metal ions.[29] In order to examine the oxidation states of nickel and cobalt ions in NCA derivatives, XAFS measurements were conducted and the Ni K-edge X-ray absorption near-edge structure (XANES) spectra are displayed in Fig. 3. The oxidation state of cobalt ions in NCA derivatives is invariable irrespective of the y values by the Co K-edge XANES spectra (Fig. S2†), which indicates that cobalt ions are as Co^{3+} in the oxidation state. As displayed in Fig. 3(a), a monotonous Ni K-edge shift to a lower energy is seen as the y value increases, indicating the reduction of nickel ions in NCA derivatives. Edge energies at a half-step height are displayed in Fig. 3(b), which are the energies at a normalized absorbance of 0.5 and are often used to estimate the oxidation state of nickel ions.[38] The NCA sample of y = 0.0023 was prepared by a lithium excess amount z > 1, and therefore the oxidation state of nickel ions is close to Ni^{3+}. The edge energy follows a descending line, which indicates that NCA derivatives having rock-salt domains are actually prepared to examine the cycling test of non-aqueous lithium cells and the cylindrical lithium-ion batteries.

Table 1 Summary on the Rietveld analysis of $Li_zNi_{0.8}Co_{0.15}Al_{0.05}O_{2-\delta}$ ($z = 0.8$–1.05) to be the structure of $[Li_{1-y}Ni_y]^{3(b)}[Ni,Co,Al]^{3(a)}O_2$ based on a space group of $R\bar{3}m$

			Lattice parameter					
z	Refined structure	$(1-y)/(1+y)$	a-Axis	c-Axis	c/a	Z_{ox}	wR_p	R_p
1.05	$[Li_{0.9977}Ni_{0.0023}]^{3(b)}[Ni_{0.7995}Co_{0.1503}Al_{0.0501}]^{3(a)}O_2$	0.995	2.864 Å	14.180 Å	4.951	0.2596	11.60	8.22
1.02	$[Li_{0.9948}Ni_{0.0052}]^{3(b)}[Ni_{0.7990}Co_{0.1508}Al_{0.0503}]^{3(a)}O_2$	0.990	2.864 Å	14.182 Å	4.952	0.2598	11.34	8.06
1.00	$[Li_{0.9907}Ni_{0.0093}]^{3(b)}[Ni_{0.7981}Co_{0.1514}Al_{0.0505}]^{3(a)}O_2$	0.982	2.865 Å	14.185 Å	4.951	0.2598	10.84	7.77
0.98	$[Li_{0.9806}Ni_{0.0194}]^{3(b)}[Ni_{0.7961}Co_{0.1529}Al_{0.0510}]^{3(a)}O_2$	0.962	2.866 Å	14.187 Å	4.950	0.2595	10.60	7.64
0.95	$[Li_{0.9627}Ni_{0.0373}]^{3(b)}[Ni_{0.7925}Co_{0.1556}Al_{0.0519}]^{3(a)}O_2$	0.928	2.867 Å	14.191 Å	4.950	0.2596	10.42	7.63
0.9	$[Li_{0.9393}Ni_{0.0607}]^{3(b)}[Ni_{0.7879}Co_{0.1591}Al_{0.0530}]^{3(a)}O_2$	0.886	2.870 Å	14.197 Å	4.947	0.2594	9.75	7.17
0.8	$[Li_{0.8720}Ni_{0.1280}]^{3(b)}[Ni_{0.7744}Co_{0.1692}Al_{0.0564}]^{3(a)}O_2$	0.773	2.876 Å	14.214 Å	4.942	0.2590	8.32	6.38

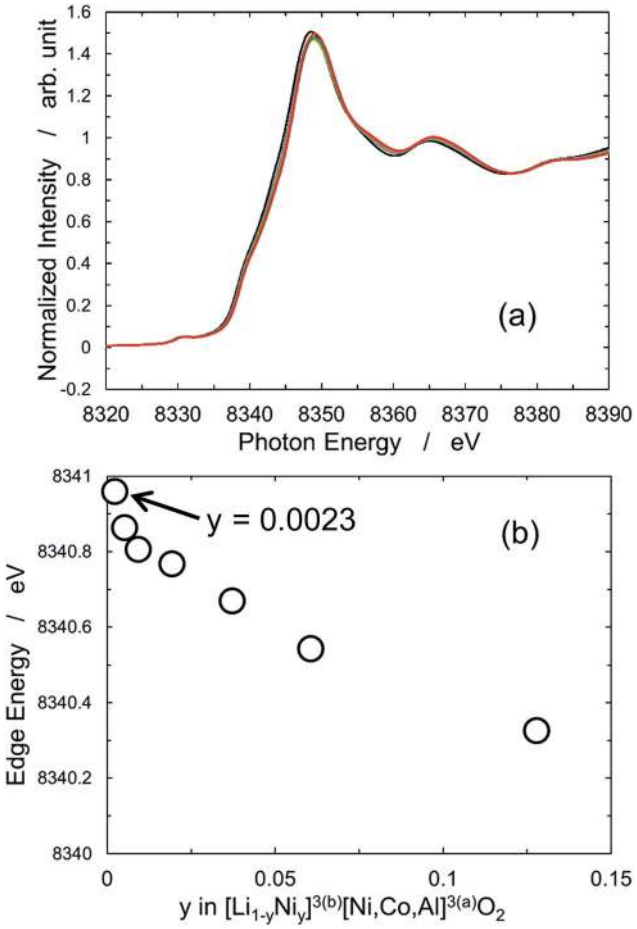

Fig. 3 (a) Ni K-edge XANES spectra of $Li_zNi_{0.8}Co_{0.15}Al_{0.05}O_{2-\delta}$ corresponding to $[Li_{1-y}Ni_y]^{3(b)}[Ni,Co,Al]^{3(a)}O_2$ based on a space group of $R\bar{3}m$. Edge energies at half-step heights as a function of the amount of rock-salt domain, y, are also displayed in (b).

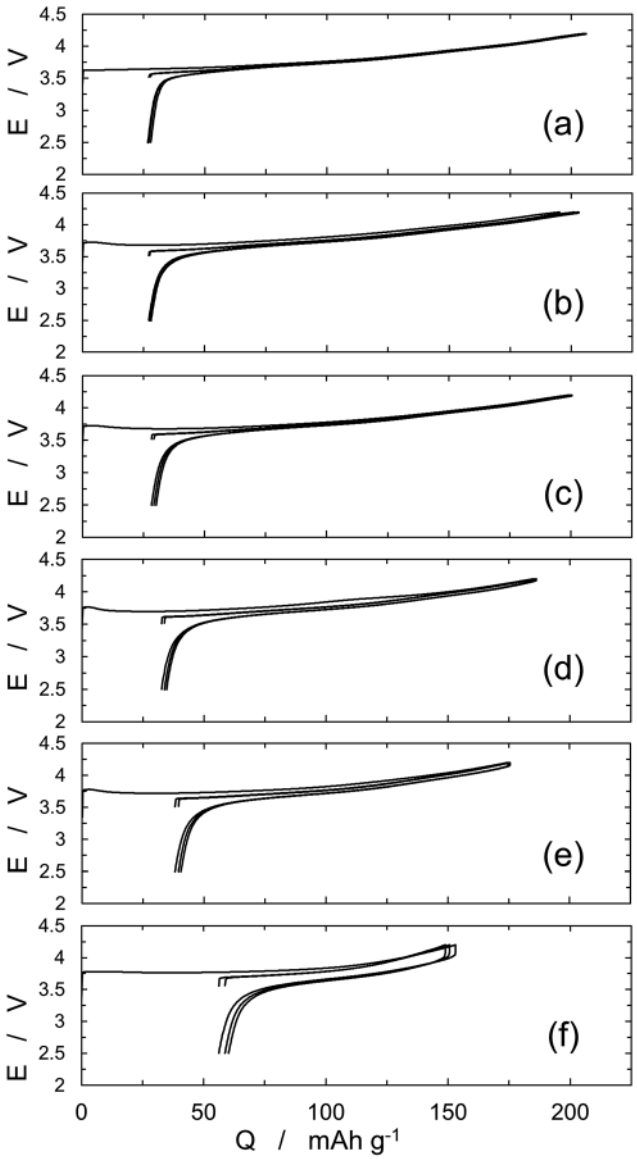

Fig. 4 Voltage profiles of lithium cells of $Li_zNi_{0.8}Co_{0.15}Al_{0.05}O_{2-\delta}$ corresponding to $[Li_{1-y}Ni_y]^{3(b)}[Ni,Co,Al]^{3(a)}O_2$ based on a space group of $R\bar{3}m$; y [z] = (a) 0.0023 [1.05], (b) 0.0093 [1.00], (c) 0.0194 [0.98], (d) 0.0373 [0.95], (e) 0.0607 [0.90], and (f) 0.1280 [0.80]. The cells were operated in a voltage window of 4.2–2.5 V at C/10-rate at 20 °C.

As described above, NCA derivatives of $Li_zNi_{0.8}Co_{0.15}Al_{0.05}O_{2-\delta}$ ($0.8 \leq z \leq 1.05$) were prepared and refined by a Rietveld method of the XRD patterns to be $[Li_{1-y}Ni_y]^{3(b)}[Ni,Co,Al]^{3(a)}O_2{}^{6(c)}$ ($0.0023 \leq y \leq 0.1280$) based on a space group of $R\bar{3}m$. Nickel ions are reduced from the oxidation state of Ni^{3+} toward Ni^{2+} in the layered structure as the y value increases. Nickel ions of Ni^{2+} in the oxidation states are incorporated into the lithium layers because of the similarity of the ionic radii between Li^+ and Ni^{2+} ions.[6,33,39]

These results indicate that the y values are the amount of rock-salt domains in NCA derivatives and the rock-salt domains correspond to the degradation of the positive electrode appearing during the extended cycling test of the cylindrical lithium-ion batteries at an elevated temperature above 60 °C.[20,21] The amount of rock-salt domains in the NCA derivatives prepared in this work was as high as 12.8%, and can be quantitatively controlled in 0.23–12.8%. These NCA derivatives were applied to examine the electrochemical reactivity in the lithium cells and the extended cycling test at 60 °C of the cylindrical lithium-ion batteries with the graphite negative electrode.

Rechargeable capacities of $LiNi_{0.8}Co_{0.15}Al_{0.05}O_2$ derivatives

In order to examine the electrochemical reactivity of the NCA derivatives with rock-salt domains in terms of a voltage profile in non-aqueous lithium cells, constant current charge and discharge measurement was performed at C/10-rate in a voltage window of 4.2–2.5 V at 20 °C. Fig. 4 displays the voltage profiles of lithium cells of NCA derivatives. The lithium cell of NCA (y = 0.0023) exhibits an ascending curve from 3.6 to 4.2 V on charge and then the discharge curve just traces the charge one in a reverse direction. The first charge and discharge capacities were 205 and 177 mA h g^{-1}, respectively, which means that a capacity of 28 mA h g^{-1} was lost during the first cycle, *i.e.*, the so-called irreversible capacity. As the amount of rock-salt domains in the NCA derivatives increases, rechargeable capacities decrease from 177 mA h g^{-1} at y = 0.0023 to about 90 mA h g^{-1} at y = 0.1280 which corresponds to capacity fading due to increased rock-salt domains. Fig. 5 shows the rechargeable capacities as a function of the y values in $[Li_{1-y}Ni_y]^{3(b)}[Ni,Co,Al]^{3(a)}O_2{}^{6(c)}$ ($0.0023 \leq y \leq 0.1280$) based on the space group of $R\bar{3}m$. A dotted line of the rechargeable capacity is drawn in the figure by assuming that the nickel ions in lithium layers are inactive. Although a linear relation between the rechargeable capacities (Q) and y values is actually seen in the figure, the obtained rechargeable capacities are smaller than the dotted line. The empirical equation is obtained to be $Q = 181.4 - 725.5y$ in which Q reaches zero at $y \approx 0.25$,

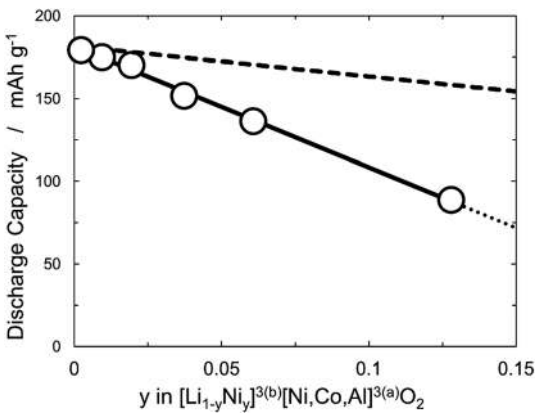

Fig. 5 Discharge capacities as a function of y in $[Li_{1-y}Ni_y]^{3(b)}$-$[Ni,Co,Al]^{3(a)}O_2$ based on a space group of $R\bar{3}m$. A dotted line was drawn by assuming that the nickel ions in lithium layers were inactive.

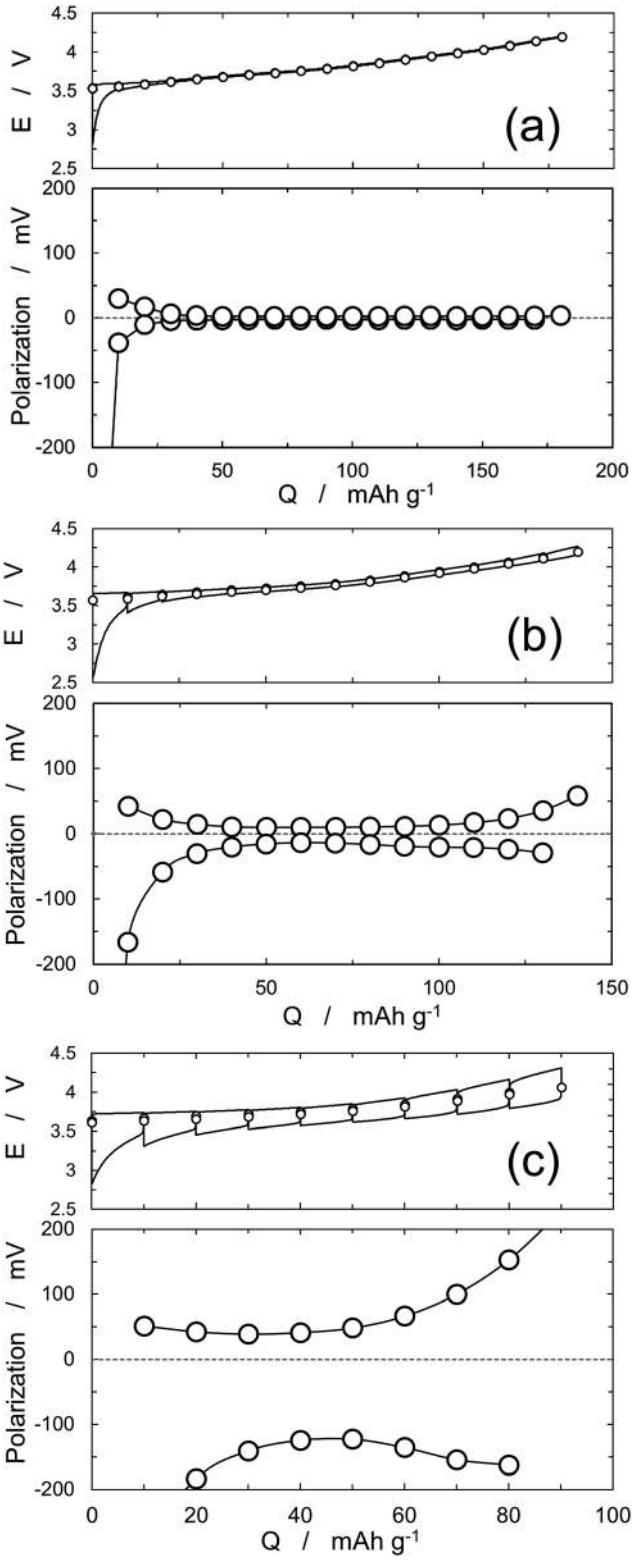

Fig. 6 Intermittent charge and discharge curves in a GITT mode of lithium cells of $[Li_{1-y}Ni_y]^{3(b)}[Ni,Co,Al]^{3(a)}O_2$ of y = (a) 0.0023, (b) 0.0607, and (c) 0.1280 at C/10-rate at 20 °C. The cell operation was interrupted every 10 mA h g^{-1}, and re-started when the voltage slope was below 1 mV h^{-1}. Polarization, defined as the difference in voltage after the lapse of 2 s to the end of the relaxation period, is also displayed. Polarization on charge is given in a positive number and that on discharge is in a negative number.

indicating that rechargeable capacities are completely lost when the nickel ions at the lithium layers increase to about 25% of NCA, which cannot be simply understood by the capacity loss derived from the increased inactive rock-salt domain in the structure. As shown in Fig. 4, decreased rechargeable capacities are associated with small first charge capacities and large irreversible capacities in the first cycle, and those are ascribed to not only to the capacity loss derived from the inactive rock-salt domain, but also the polarization increase which is shown in the voltage profiles as the large difference in operating voltage between the charge and discharge operations.

Change in polarization of $LiNi_{0.8}Co_{0.15}Al_{0.05}O_2$ derivatives during charge and discharge

The impedance spectrum for NCA electrodes with a counter electrode of lithium metal includes the impedance behavior of the lithium metal electrode.[40] In our group, the cylindrical lithium-ion batteries of NCA with graphite or the symmetric cells of two identical electrodes prepared at the same potential were fabricated and their EIS measurements were performed to examine the change in impedance of the positive and/or negative electrodes.[19,20,27,40,41] In this paper, lithium-ion mobility in the bulk structure rather than the reaction at the interface was examined by the intermittent charge and discharge measurement of lithium cells of NCA derivatives in a galvanostatic intermittent titration technique (GITT) mode.[42–44] Fig. 6 displays voltage profiles of the NCA derivatives of $y = 0.0023$, 0.0607, and 0.1280, and their polarization is defined as the difference in voltage after the lapse of 2 s to the end of the relaxation period, which is associated with mass transfer since ohmic and charge-transfer resistance appear in a short time within 2 s. As shown in Fig. 6(a), polarization of NCA ($y = 0.0023$) is quite small with 2.3–3.4 mV on both charge and discharge over the entire range of the cell operation. Increased polarization is seen at the low voltage region of about 3.5–3.6 V on both charge and discharge. A NCA derivative with increased rock-salt domains ($y = 0.0607$) exhibits larger polarization than that of NCA ($y = 0.0023$) especially at the end of charge or discharge, which draws U-shaped curves of polarization. Such degradation in electrochemical reactivity drawing U-shaped curves of polarization is more obvious in a NCA derivative having the largest amount of rock-salt domains ($y = 0.1280$). Fig. 6(c) clearly shows increased polarization at the end of charge or discharge, and polarization on discharge is larger than that on charge over the entire range of the cell operation. At the end of charge, increased polarization is one of the reasons of the decrease in rechargeable capacities as a function of the amount of rock-salt domains, and at the end of discharge, large polarization is characteristic of the appearance of the irreversible capacity seen in the first cycle.

In order to examine the electrochemical reactivity in the irreversible region, intermittent charge and discharge operation of NCA ($y = 0.0023$) was continued through the irreversible region and the voltage profile is shown in Fig. S3.† The open-circuit voltages on discharge in the irreversible region are the same as those on charge, and the cell can be discharged back to the initial 0 mA h g^{-1}, which indicates that the irreversible capacity in the first cycle can be recovered by an intermittent mode. Fig. S4† displays the voltage profiles of NCA ($y = 0.0023$) operated in a 200 mA h g^{-1} capacity-limited mode at 20, 60, and 80 °C. Although NCA exhibits 25 mA h g^{-1} of the irreversible capacity at 20 °C, this can be recovered with low voltage discharge below 2.0 V. As shown in Fig. S4,† the so-called irreversible capacity shrinks from 25 mA h g^{-1} at 20 °C to below 10 mA h g^{-1} at elevated temperature. These results indicate that the irreversible capacity is under kinetic control. Fig. 7 displays the crystal structure of a NCA derivative with rock-salt domains. The mechanisms of the irreversible capacity have been proposed by several research groups, and have been discussed from a viewpoint of lithium ion mobility in the crystal structure. Delmas *et al.* proposed the mechanism associated with Ni^{2+} ions placed in the lithium layers.[33] During the first charge, the Ni^{2+} ions in the lithium layers oxidize to smaller Ni^{3+} ions, which induce a local collapse in the structure. The local collapse makes it difficult to insert lithium ions back to the structure. Ceder *et al.* discussed lithium ion mobility in terms of monovacancy or divacancy hopping associated with an interlayer distance in the layered structure,

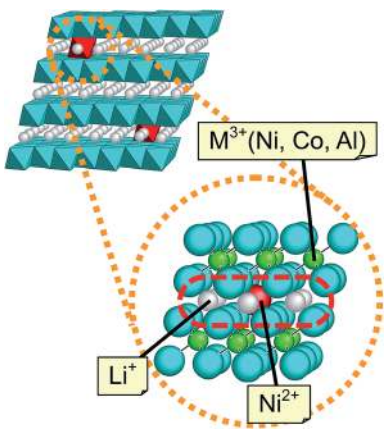

Fig. 7 Nickel ions at the lithium sheets in a layered structure of $[Li_{1-y}Ni_y]^{3(b)}[Ni,Co,Al]^{3(a)}O_2$ based on a space group of $R\bar{3}m$.

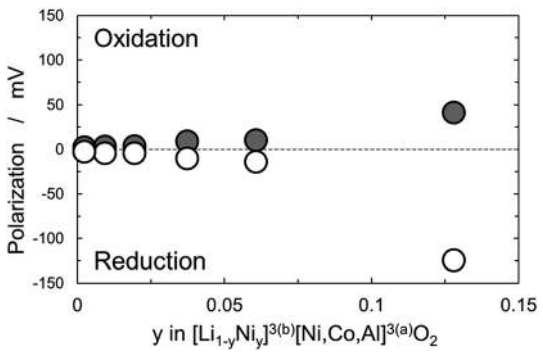

Fig. 8 Polarization at the midpoint of rechargeable capacity as a function of y in $[Li_{1-y}Ni_y]^{3(b)}[Ni,Co,Al]^{3(a)}O_2$ obtained by GITT experiments at C/10-rate at 20 °C.

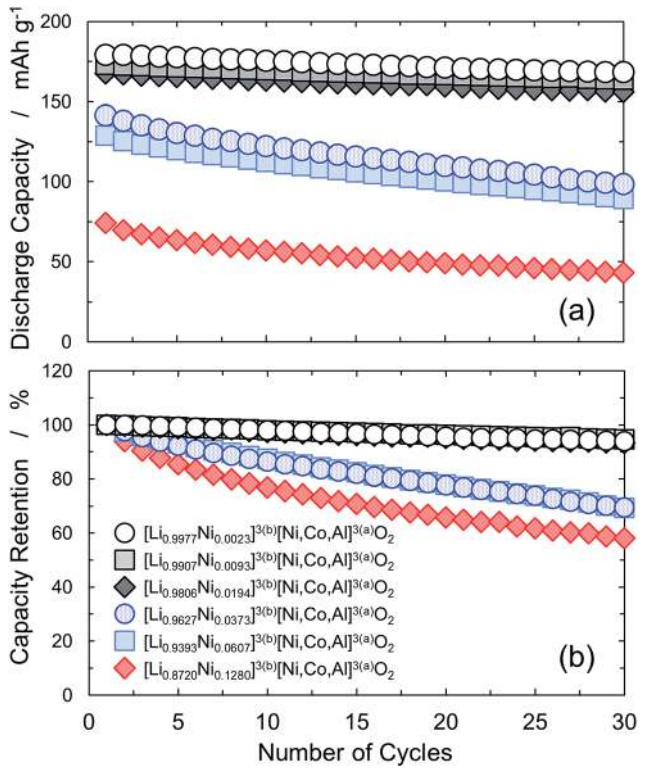

Fig. 9 (a) Discharge capacities and (b) capacity retentions for the lithium cells of $[Li_{1-y}Ni_y]^{3(b)}[Ni,Co,Al]^{3(a)}O_2$ based on a space group of $R\bar{3}m$ operated in a voltage window of 4.2–2.5 V at C/10-rate at 20 °C.

and then Dahn *et al.* and Kang *et al.* discussed the irreversible capacity on the basis of the results on Ceder's calculation.[45–49] Our results on the irreversible capacity displayed in Fig. S3 and S4† strongly suggest that the irreversible capacity is derived from kinetic limitation of lithium insertion into the structure. According to the relation between the increased irreversible capacity at the end of discharge and the polarization increase over the entire range of the operation, the increased polarization of the NCA derivatives with a large amount of rock-salt domains especially in the discharge direction or lithium insertion direction into the structure are mainly derived from slow lithium ion mobility due to the nickel ions in the lithium layers.

Fig. 8 shows polarization of NCA derivatives at the midpoint of the rechargeable capacity as a function of the y values in $[Li_{1-y}Ni_y]^{3(b)}[Ni,Co,Al]^{3(a)}O_2{}^{6(c)}$ based on the space group of $R\bar{3}m$. Polarization of NCA derivatives on discharge corresponding to lithium insertion into the structure is larger than that on charge. According to the results on the irreversible capacity, increased polarization of the NCA derivatives with rock-salt domains especially in the discharge direction is ascribed to slow lithium ion mobility due to the rock-salt domains. Polarization increases when the amount of rock-salt domains is above 2%, *i.e.*, $y > 0.02$, and the largest amount of 12.8% of rock-salt domains among the NCA derivatives examined causes the largest polarization of 41 mV on charge and 125 mV on discharge.

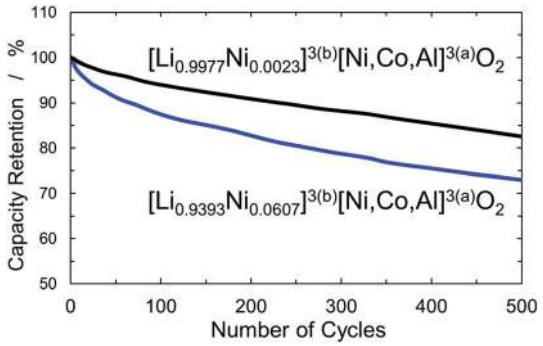

Fig. 10 Capacity retention for the 500 mA h class cylindrical lithium-ion batteries of $y = 0.0023$ and 0.0607 in $[Li_{1-y}Ni_y]^{3(b)}[Ni,Co,Al]^{3(a)}O_2$ with a graphite negative electrode operated in a voltage window of 4.1–3.0 V at 2C-rate at 60 °C.

Charge and discharge cycling stability of $LiNi_{0.8}Co_{0.15}Al_{0.05}O_2$ derivatives in lithium cells or cylindrical lithium-ion batteries with a graphite negative electrode

In order to examine the cumulative increase in polarization of the NCA derivatives during charge and discharge cycles, the cycling test of lithium cells of the NCA derivatives was performed at a low rate of C/10 at 20 °C. This measurement is appropriate to examine materials degradation since the materials are exposed in a charged state at high voltage for almost a month and other factors of battery deterioration can be excluded. Fig. 9 displays discharge capacities and capacity retentions of lithium cells of the NCA derivatives. As shown in Fig. 9(a), discharge capacities decrease as the amount of rock-salt domains increases. Of these, discharge capacities of the NCA derivatives in $y < 0.02$ draw parallel lines during 30 cycles. This means that the capacity retentions are almost the same values of 93–95% in 30 cycles for the samples having rock-salt domains of below 2% as shown in Fig. 9(b). Capacity retentions decrease to 69–70% when the amount of rock-salt domains exceeds 2%. The NCA derivative having the largest amount of 12.8% of rock-salt domains exhibits the lowest capacity retention of 58% for 30 cycles among the NCA derivatives. There seems to be a one-to-one correspondence between the capacity retentions for 30 cycles and the amount of rock-salt domains in terms of the increased polarization examined by GITT measurement associated with the slow lithium ion mobility derived from the rock-salt domains.

Such a polarization increase during cycling is also superposed on the extended cycling test for the cylindrical lithium-ion batteries at an elevated temperature of 60 °C. The NCA derivatives of $y = 0.0023$ and 0.0607 were chosen to fabricate the cylindrical lithium-ion batteries with a graphite negative electrode because they exhibited the characteristic capacity retentions in the lithium cells for 30 cycles. The extended cycling test for the cylindrical lithium-ion batteries were performed for 500 cycles at 2C-rate at an elevated temperature of 60 °C. Fig. 10 displays the capacity retentions of the cylindrical lithium-ion batteries for 500 cycles. NCA of $y = 0.0023$ gives 83% capacity retention in the cylindrical lithium-ion battery after 500 cycles

at 60 °C, and the capacity retention of the NCA derivative of $y = 0.0607$ in the cylindrical battery is 73%, which is lower than that of NCA. Battery deterioration derived from materials degradation of NCA is accelerated when the NCA derivatives have a large amount of rock-salt domains. Increased polarization during cycling due to nickel ions at the lithium layers is the main factor affecting the accelerated deterioration of cycling life. These results on the NCA derivatives strongly suggest that the materials innovation to prevent the formation of rock-salt domains will improve the cycling life of the cylindrical lithium-ion batteries at elevated temperature. Substitution of metal ions of lower oxidation states such as Mg^{2+} for nickel ions in NCA, which can act to increase the oxidation state of nickel ions, is one of the effective ways to improve battery performance. A part of our research works has been reported in our previous papers.[10,19,27,50]

Conclusions

NCA derivatives of $Li_zNi_{0.8}Co_{0.15}Al_{0.05}O_{2-\delta}$ $(0.8 \leq z \leq 1.05)$ or $[Li_{1-y}Ni_y]^{3(b)}[Ni,Co,Al]^{3(a)}O_2{}^{6(c)}$ based on a space group of $R\bar{3}m$, in which the y value is the amount of rock-salt domains, were prepared by adjusting the Li/(Ni, Co, Al) ratios and electrochemical measurements in non-aqueous lithium cells were performed to clarify the relation between the amount of rock-salt domains and electrochemical reactivity in terms of rechargeable capacity and polarization. The rechargeable capacities of NCA derivatives in non-aqueous lithium cells decrease linearly as a function of the y value and reach zero at $y \approx 0.25$ by extrapolating the straight line. Such a relation is derived from not only the lost capacity due to inactive rock-salt domains but the increased polarization. GITT measurement told us that nickel ions at the lithium layers in NCA of above 2% cause a polarization increase especially during discharge operation or of lithium insertion into the structure, which is ascribed to slow lithium ion mobility due to nickel ions in the lithium layers. The low rate cycling test of non-aqueous lithium cells of NCA derivatives indicated that the accelerated capacity fading is associated with the increased polarization. The extended cycling test of the cylindrical lithium-ion batteries with a graphite negative electrode at an elevated temperature of 60 °C indicated that the rock-salt domains in NCA cause and accelerate further degradation. Materials innovation to prevent the formation of rock-salt domains will be an effective way to improve the cycling life of lithium-ion batteries at elevated temperature. Substitution of Mg^{2+} ions for nickel ions in NCA will be discussed with respect to rechargeable capacity, polarization, and capacity retention in our forthcoming papers.

Conflict of interest

The authors declare no competing financial interest.

Acknowledgements

The authors wish to thank Mr Yasuhito Kondo for ICP-AES measurements and Mr Juntaro Seki for SEM observations. The synchrotron radiation experiments were performed at the BL33XU of SPring-8 with the approval of the Japan Synchrotron Radiation Research Institute (JASRI) (Proposal No. 2014A7008 and 2014B7008).

References

1 M. S. Whittingham, *Chem. Rev.*, 2004, **104**, 4271.
2 T. Ohzuku and R. J. Brodd, *J. Power Sources*, 2007, **174**, 449.
3 B. L. Ellis, K. T. Lee and L. F. Nazar, *Chem. Mater.*, 2010, **22**, 691.
4 V. Etacheri, R. Marom, R. Elazari, G. Salitra and D. Aurbach, *Energy Environ. Sci.*, 2011, **4**, 3243.
5 T. Ohzuku, A. Ueda and M. Nagayama, *J. Electrochem. Soc.*, 1993, **140**, 1862.
6 C. Delmas, M. Ménétrier, L. Croguennec, I. Saadoune, A. Rougier, C. Pouillerie, G. Prado, M. Grüne and L. Fournès, *Electrochim. Acta*, 1999, **45**, 243.
7 S. Tobishima and J. Yamaki, *J. Power Sources*, 1999, **81–82**, 882.
8 R. A. Leising, M. J. Palazzo, E. S. Takeuchi and K. J. Takeuchi, *J. Electrochem. Soc.*, 2001, **148**, A838.
9 T. Ohsaki, T. Kishi, T. Kuboki, N. Takami, N. Shimura, Y. Sato, M. Sekino and A. Satoh, *J. Power Sources*, 2005, **146**, 97.
10 T. Sasaki, V. Godbole, Y. Takeuchi, Y. Ukyo and P. Novák, *J. Electrochem. Soc.*, 2011, **158**, A1214.
11 S. Watanabe, M. Kinoshita, T. Hosokawa, K. Morigaki and K. Nakura, *J. Power Sources*, 2014, **258**, 210.
12 S. Watanabe, M. Kinoshita, T. Hosokawa, K. Morigaki and K. Nakura, *J. Power Sources*, 2014, **260**, 50.
13 K. Amine, C. H. Chen, J. Liu, M. Hammond, A. Jansen, D. Dees, I. Bloom, D. Vissers and G. Henriksen, *J. Power Sources*, 2001, **97–98**, 684.
14 J. Shim, R. Kostecki, T. Richardson, X. Song and K. A. Striebel, *J. Power Sources*, 2002, **112**, 222.
15 D. P. Abraham, R. D. Twesten, M. Balasubramanian, I. Petrov, J. McBreen and K. Amine, *Electrochem. Commun.*, 2002, **4**, 620–625.
16 D. P. Abraham, R. D. Twesten, M. Balasubramanian, J. Kropf, D. Fischer, J. McBreen, I. Petrov and K. Anine, *J. Electrochem. Soc.*, 2003, **150**, A1450.
17 Y. Itou and Y. Ukyo, *J. Power Sources*, 2005, **146**, 39.
18 R. Kostecki, J. Lei, F. McLarnon, J. Shim and K. Striebel, *J. Electrochem. Soc.*, 2006, **153**, A669.
19 H. Kondo, Y. Takeuchi, T. Sasaki, S. Kawauchi, Y. Itou, O. Hiruta, C. Okuda, M. Yonemura, T. Kamiyama and Y. Ukyo, *J. Power Sources*, 2007, **174**, 1131.
20 T. Sasaki, T. Nonaka, H. Oka, C. Okuda, Y. Itou, Y. Kondo, Y. Takeuchi, Y. Ukyo, K. Tatsumi and S. Muto, *J. Electrochem. Soc.*, 2009, **156**, A289.
21 S. Muto, Y. Sasano, K. Tatsumi, T. Sasaki, K. Horibuchi, Y. Takeuchi and Y. Ukyo, *J. Electrochem. Soc.*, 2009, **156**, A371.
22 T. Hayashi, J. Okada, E. Toda, R. Kuzuo, N. Oshimura, N. Kuwata and J. Kawamura, *J. Electrochem. Soc.*, 2014, **161**, A1007.

23 Y. Makimura, C. Okuda, T. Nonaka, Y. F. Nishimura, T. Sasaki and Y. Takeuchi, *ECS Electrochem. Lett.*, 2014, **3**, A66.
24 M. Guilmard, L. Croguennec, D. Denux and C. Delmas, *Chem. Mater.*, 2003, **15**, 4476.
25 M. Guilmard, L. Croguennec and C. Delmas, *Chem. Mater.*, 2003, **15**, 4484.
26 H.-J. Bang, H. Joachin, H. Yang, K. Amine and J. Prakash, *J. Electrochem. Soc.*, 2006, **153**, A731.
27 S. Muto, K. Tatsumi, Y. Kojima, H. Oka, H. Kondo, K. Horibuchi and Y. Ukyo, *J. Power Sources*, 2012, **205**, 449.
28 B. H. Toby, *J. Appl. Crystallogr.*, 2001, **34**, 210.
29 A. Rougier, P. Gravereau and C. Delmas, *J. Electrochem. Soc.*, 1996, **143**, 1168.
30 S. Zheng, R. Huang, Y. Makimura, Y. Ukyo, C. A. J. Fisher, T. Hirayama and Y. Ikuhara, *J. Electrochem. Soc.*, 2011, **158**, A357.
31 Y. Makimura, S. Zheng, Y. Ikuhara and Y. Ukyo, *J. Electrochem. Soc.*, 2012, **159**, A1070.
32 T. Ohzuku, A. Ueda, M. Nagayama, Y. Iwakoshi and H. Komori, *Electrochim. Acta*, 1993, **38**, 1159.
33 C. Delmas, J. P. Pérès, A. Rougier, A. Demourgues, F. Weill, A. Chadwick, M. Broussely, F. Perton, Ph. Biensan and P. Willmann, *J. Power Sources*, 1997, **68**, 120.
34 B. Ammundsen and J. Paulsen, *Adv. Mater.*, 2001, **13**, 943.
35 T. Ohzuku, K. Ariyoshi, Y. Makimura, N. Yabuuchi and K. Sawai, *Electrochemistry*, 2005, **73**, 2.
36 M. M. Thackeray, S.-H. Kang, C. S. Johnson, J. T. Vaughey, R. Benedek and S. A. Hackney, *J. Mater. Chem.*, 2007, **17**, 3112.
37 T. Ohzuku and Y. Makimura, *Res. Chem. Intermed.*, 2006, **32**, 507.
38 A. N. Mansour and C. A. Melendres, *J. Phys. Chem. A*, 1998, **102**, 65.
39 R. D. Shannon, *Acta Crystallogr., Sect. A: Cryst. Phys., Diffr., Theor. Gen. Crystallogr.*, 1976, **32**, 751.
40 N. Ogihara, S. Kawauchi, C. Okuda, Y. Itou, Y. Takeuchi and Y. Ukyo, *J. Electrochem. Soc.*, 2012, **159**, A1034.
41 N. Ogihara, Y. Itou, T. Sasaki and Y. Takeuchi, *J. Phys. Chem. C*, 2015, **119**, 4612.
42 W. Weppner and R. A. Huggins, *J. Electrochem. Soc.*, 1977, **124**, 1569.
43 D. W. Dees, S. Kawauchi, D. P. Abraham and J. Prakash, *J. Power Sources*, 2009, **189**, 263.
44 R. Amin, D. B. Ravnsbæk and Y.-M. Chiang, *J. Electrochem. Soc.*, 2015, **162**, A1163.
45 A. Van der Ven and G. Ceder, *Electrochem. Solid-State Lett.*, 2000, **3**, 301.
46 J. R. Mueller-Neuhaus, R. A. Dunlap and J. R. Dahn, *J. Electrochem. Soc.*, 2000, **147**, 3598.
47 A. Van der Ven and G. Ceder, *J. Power Sources*, 2001, **97–98**, 529.
48 K. Kang and G. Ceder, *Phys. Rev. B: Condens. Matter Mater. Phys.*, 2006, **74**, 094105.
49 S.-H. Kang, W.-S. Yoon, K.-W. Nam, X.-Q. Yang and D. P. Abraham, *J. Mater. Sci.*, 2008, **43**, 4701.
50 K. Tatsumi, Y. Sasano, S. Muto, T. Yoshida, T. Sasaki, K. Horibuchi, Y. Takeuchi and Y. Ukyo, *Phys. Rev. B: Condens. Matter Mater. Phys.*, 2008, **78**, 045108.